crystals

MDPI

Article

Luminescence and Scintillation Properties of $YAl_3(BO_3)_4$ Single Crystal for Thermal Neutron Detection

Yutaka Fujimoto [1,*], Masanori Koshimizu [2], Hiroki Kawamoto [1], Kenichi Watanabe [3], Akio Miyamoto [4] and Keisuke Asai [1]

[1] Department of Applied Chemistry, Graduate School of Engineering, Tohoku University, 6-6-07 Aramaki Aza Aoba, Aoba-ku, Sendai 980-8579, Miyagi, Japan
[2] Research Institute of Electronics, Shizuoka University, 3-5-1 Johoku, Naka-ku, Hamamatsu 432-8011, Shizuoka, Japan
[3] Faculty of Engineering, Kyushu University, 744 Motooka, Nishi-ku, Hamamatsu 432-8011, Shizuoka, Japan
[4] OXIDE Corporation, 1747-1 Maginohara, Mukawa, Hokuto 408-0302, Yamanashi, Japan
* Correspondence: yutaka.fujimoto.c3@tohoku.ac.jp; Tel.: +81-22-795-7219

Abstract: A single crystal of $YAl_3(BO_3)_4$ was grown using the top-seeded solution growth method. The vacuum ultraviolet (VUV) excitation spectrum, monitored at the emission wavelength of 312 and 372 nm, showed a narrow excitation band at around 162 nm, which is located near the absorption edge of the $YAl_3(BO_3)_4$ host. Upon VUV excitation at 162 nm, the characteristic self-trapped exciton (STE) emission bands were observed at 312 and 372 nm. The X-ray excited scintillation spectrum shows a broad emission band peaking at 310 nm with a weak shoulder band at around 375 nm, which is consistent with photoluminescence, and can thus be assigned to the STE emission. The scintillation light yield under irradiation at a ^{252}Cf-thermal neutron reached 2700 photons/thermal neutron.

Keywords: scintillator; borate; thermal neutron; self-trapped excitons (STEs)

check for updates

Academic Editor: Zongyou Yin

Received: 19 March 2025
Revised: 8 April 2025
Accepted: 10 April 2025
Published: 12 April 2025

Citation: Fujimoto, Y.; Koshimizu, M.; Kawamoto, H.; Watanabe, K.; Miyamoto, A.; Asai, K. Luminescence and Scintillation Properties of $YAl_3(BO_3)_4$ Single Crystal for Thermal Neutron Detection. *Crystals* **2025**, *15*, 357. https://doi.org/10.3390/cryst15040357

Copyright: © 2025 by the authors. Licensee MDPI, Basel, Switzerland. This article is an open access article distributed under the terms and conditions of the Creative Commons Attribution (CC BY) license (https://creativecommons.org/licenses/by/4.0/).

1. Introduction

A scintillator generates ultraviolet (UV) or visible photons in response to the incident radiation which can be detected by a photo-sensitive detector such as a photomultiplier tube (PMT) and photodiode (PD) to estimate the energy deposited in the scintillation detector by the radiation. Generally, the incident radiation includes high-energy photons and particles such as X-rays, gamma-rays, alpha particles, beta particles, and neutrons. Thus, a variety of scintillators are being designed for radiation detection because different types of ionizing radiation interact with matters. Among other radiation detection techniques expected for the scintillation detector, the type of gaseous ionization detector such as a proportional counter can be mentioned. Helium-3 (^{3}He) has various applications as a gold standard proportional counter for neutron detection due to the ^{3}He(n, p)^{3}H reaction (Q = 0.765 MeV, σ_{abs} = 5330 barns) for national security purposes, nuclear safeguards measurements, neutron scattering facilities, oil and gas exploration, and Boron Neutron Capture Therapy (BNCT) [1–6]. It is also important in cryogenics including low-temperature physics research and quantum computing, and increasingly in medical diagnostics. However, the ^{3}He supply has recently been significantly limited despite the increasing demand for its use in the neutron detector worldwide. For the reasons mentioned above, continuous study of alternative thermal neutron detectors is strongly required. One of the candidate technologies is a scintillation detector consisting of lithium-6 (^{6}Li)- and a boron-10 (^{10}B)-based scintillator that is optically coupled to a photosensitive detector because both ^{6}Li and ^{10}B have large

neutron capture cross-sections (^{6}Li: 940 barns, ^{10}B: 3840 barns) [1]. The ^{6}Li(n, α)^{3}H reaction releases 4.78 MeV of energy (Q-value), which is distributed as 2.05 MeV to the alpha particle and 2.73 MeV to the triton; meanwhile, the natural abundance of ^{6}Li is only 7.5%. Many ^{6}Li(n, α)^{3}H reaction-based inorganic scintillators with a good performance including LiI_2:Eu [7], Li-glass [8], $LiBaF_3$ [9], $LiCaAlF_6$:Eu [10], $LiCaAlF_6$:Ce [11], LiF-CaF_2 [12], LiF-CaF_2:Eu [13], $LiAlO_2$ [14,15], $LiGaO_2$ [15], Cs_2LiYCl_6:Ce [16], Tl_2LiYCl_6:Ce [17], LiF:W [18], NaI:Tl, Li [19], Li-$(PEA)_2PbBr_4$ [20], LiI:Ag [21], Ce:$Li_6Y(BO_3)_3$ [22], and $Cs_3Cu_2I_5$:Li [23] have been reported thus far. Among the scintillators, $LiCaAlF_6$:Eu, $LiCaAlF_6$:Ce, and Cs_2LiYCl_6:Ce are now commercially available. In the ^{10}B(n, α)^{7}Li reaction, 94% of the reactions produce the 1.47 MeV alpha particle and 0.84 MeV ^{7}Li, and that of 6% produce the 1.78 MeV alpha particle and 1.01 MeV ^{7}Li. Despite the larger neutron capture cross-section and a relatively high natural abundance (~19.9%) when compared to ^{6}Li, the number of reports about ^{10}B(n, α)^{7}Li reaction-based scintillators is quite small on a global scale. Although BF_3 gas-filled detectors have also been extensively utilized for thermal neutron detection, the inherent corrosiveness and toxicity of BF_3 present significant safety and operational challenges [24,25]. Hence, there is a need for more research into alternative thermal neutron detectors based on ^{0}B-based scintillators. This study focused on yttrium aluminum borate $YAl_3(BO_3)_4$ as a novel neutron scintillator host because it contains a considerable amount of boron. $YAl_3(BO_3)_4$ was discovered in the 1960s [26,27] and it belongs to the carbonate huntite-type structure in the space group of *R*32. Notably, while $YAl_3(BO_3)_4$ possesses high hardness (Mohs 7.5), favorable physical properties, and chemical stability, its Y^{3+} site is easily replaceable by trivalent rare-earth ions. Therefore, the YAB single crystals activated with rare-earth ions have attracted great interest for application in laser, nonlinear optical, and phosphor material [28–35]. Aloui-Lebbou et al. previously reported that an additional emission band peaking at 300 nm was observed in Ce^{3+}-doped $YAl_3(BO_3)_4$ powder under excitation at X-ray, which is an intrinsic emission due to a self-trapped exciton (STE) [35]. A similar intrinsic emission band under-excited at an ionizing radiation was confirmed in the study of some borate crystals [36–40]. In particular, calcium metaborate CaB_2O_4 showed an intense intrinsic emission band peaking at around 300–400 nm and a scintillation light yield under-irradiated at a thermal neutron reached approximately 3200 photons/thermal neutron [38]. In this study, we examined the photoluminescence and scintillation properties of an undoped $YAl_3(BO_3)_4$ single crystal with an expectation of efficient intrinsic emission owing to the STE for the neutron detector. Considering the existing industrial availability of the YAB crystals for laser applications, the successful demonstration of their neutron scintillation capabilities in this research could lead to an expedited practical implementation.

2. Materials and Methods

The single crystal sample of $YAl_3(BO_3)_4$ was prepared in an 80 mm diameter platinum crucible provided by the OXIDE Corporation via the conventional top-seeded solution growth method with a Li_2O-Al_2O_3-B_2O_3 flux under an atmosphere of N_2 + 3% H_2. High-purity powders of Y_2O_3 (5N), Al_2O_3 (4N), B_2O_3 (5N), and Li_2CO_3 (4N) were used as raw materials for the crystal growth. The transmittance spectrum in the wavelength ranges from 190 to 800 nm was measured using a UV-2700 spectrometer (SHIMADZU, Kyoto, Japan). The intrinsic emission properties were investigated through the use of vacuum ultraviolet (VUV) light as an excitation source. The excitation and emission spectrum measurements were performed at beamline 7B of the Universal Virtual Spectroscope for Optoelectronics Research (UVSOR) facility at the Institute for Molecular Science, Okazaki, Japan [41,42]. The sample was irradiated with a monochromated VUV light, and the fluorescence photons from the sample were detected using a spectroscopic system consisting of a charged-

coupled device (CCD) detector and a monochromator in a vacuum chamber. The excitation wavelength is in the VUV region from 50 to 200 nm. The scintillation spectrum was measured under continuous irradiation from a SA-HFM3 X-ray generator (Rigaku Holdings Corp., Tokyo, Japan) operating at 40 kV and 40 mA. The scintillation photons from the sample were recorded from 200 nm to 700 nm by a QE Pro spectrometer (Ocean Insight, Inc., Orlando, FL, USA) that was cooled using a thermoelectric cooler (TEC). The scintillation pulse height spectra under-irradiated at 5.5 MeV alpha-rays from a ^{241}Am, 662 keV gamma-rays from a ^{137}Cs, and thermal neutron from a ^{252}Cf sealed sources were measured using the sample optically coupled to an R7600U-200 photomultiplier tube (PMT, Hamamatsu Photonics K.K.). Details of the experimental setup were reported previously in Ref. [43]. The scintillation photons were recorded with shaping times of 10 μs for $YAl_3(BO_3)_4$, 2 μs for $Bi_4Ge_3O_{12}$ (BGO, CASTECH Inc., light yield = ~8500 ph/MeV [44]), and 0.5 μs for Li-glass (GS20, Saint-Gobain, light yield = ~6000 ph/nth [45]), where the latter were used as a reference sample to estimate the light yield.

3. Results

A photograph of the as-grown $YAl_3(BO_3)_4$ crystal is shown in Figure 1a. The crystal seems to be highly transparent and colorless; this is followed by a discussion of the transmittance spectrum measurement. Part of the as-grown crystal was cut and polished optically to dimensions of 5.0 × 3.0 × 1.0 mm^3 for the optical and scintillation measurements as described below. The optical transmittance spectrum is shown in Figure 1b. The spectrum exhibited more than 75% transmittance, and no absorption bands in this wavelength were detected. This suggests that the grown crystal is of high purity and good quality. The cutoff wavelength in the crystal cannot be confirmed in this wavelength because of its large bandgap energy (~7.32 eV) [31]. Yu et al. previously reported that the cutoff wavelength for $YAl_3(BO_3)_4$ is about 170 nm by using a VUV spectrophotometer [46], which is in agreement with our result.

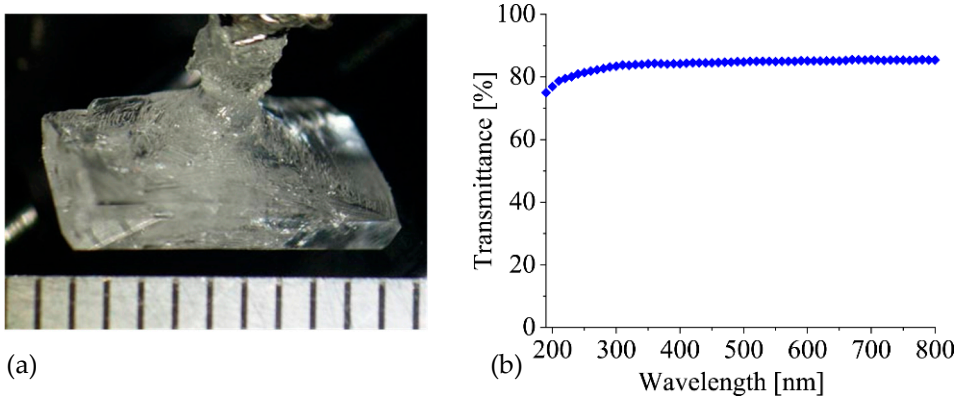


Figure 1. (**a**) Photograph of as-grown $YAl_3(BO_3)_4$ single crystal and (**b**) optical transmittance spectrum of the polished crystal sample.

The excitation and emission spectra of $YAl_3(BO_3)_4$ are shown in Figure 2. The excitation spectra with an emission wavelength of 312 and 372 nm showed a narrow excitation band at about 162 nm. Considering the bandgap energy of ~7.32 eV for $YAl_3(BO_3)_4$, the narrow excitation band is located around the bandgap. A similar excitation band from the $YAl_3(BO_3)_4$:Dy^{3+}, $YAl_3(BO_3)_4$:Ce^{3+}, and $YAl_3(BO_3)_4$ was reported [30,33,35], which is due to the absorption of the host crystal, resulting in the formation of electron-hole pairs like excitons. Yoshida et al. discussed the electronic structure of $YAl_3(BO_3)_4$ with a first-principles molecular orbital method using the refined crystal structure [31]. The electronic structure calculations show that the valence band of $YAl_3(BO_3)_4$ is primarily formed by the

O 2p state, whereas the conduction band edge is typically a complex mixture of B 2p and Y 4d states. Therefore, the excitation band near the bandgap energy is attributed to optical transitions from the O 2p state to the complex B 2p-Y 4d states. A similar excitation band has been confirmed by previously reports about $YAl_3(BO_3)_4$ powder samples synthesized by a solid-state reaction [31]. The emission spectrum excited at 162 nm showed a major emission band at 312 nm with a sub band at 372 nm. The Stokes shift can be calculated to be about 29,680 cm^{-1} for 312 nm and 34,851 cm^{-1} for 372 nm. Yokosawa et al. and Yoshida et al. reported these intrinsic emission bands from some borate compounds such as $La(BO_2)_3$, $LaMgB_5O_{10}$, YBO_3, and $YAl_3(BO_3)_4$ and suggested that the origins of these emission bands are due to different BO_3 units in the crystal host [31,47]. In the case of the $YAl_3(BO_3)_4$, there are two kinds of BO_3 units ($B(1)O_3$ and $B(2)O_3$) within a unit cell. The $B(1)O_3$ units exhibit an equilateral triangular geometry, whereas the $B(2)O_3$ units adopt an isosceles triangular configuration. Therefore, considering the emission and structural characteristics, previous reports concluded that the origin of the emission band peaking at 312 nm and 372 nm is due to the STE related to the $B(1)O_3$ and $B(2)O_3$ units.

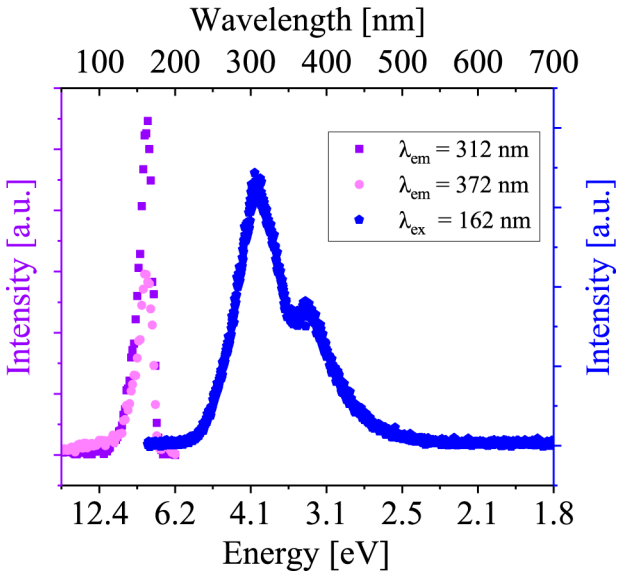


Figure 2. Excitation (purple and pink plots) and emission (blue plots) spectra of the $YAl_3(BO_3)_4$ single crystal at room temperature.

The scintillation spectrum of $YAl_3(BO_3)_4$ at 300 K along with the fitted function is shown in Figure 3a. The spectrum can be roughly fitted with sums of two Gaussian functions centered at 317 and 370 nm. This result is consistent with the spectrum under-excited at VUV lights that the dominant emission bands are assigned to the STEs which is strongly dependent on the two kinds of BO_3 units ($B(1)O_3$ and $B(2)O_3$). Figure 3b shows the scintillation spectra at different temperatures in the ranges from 11 to 300 K. There was no clear change in the spectral peak position; meanwhile, the scintillation intensity of the bands at around 317 nm (STE-1) and 370 nm (STE-2) seems to depend on the temperature. The integral intensities of the two STE bands were derived from a two-Gaussian fit to the scintillation spectra as a function of photon energy. Figure 3c shows the temperature dependence between 11 and 300 K of the STE-1 band intensity (pink circle), the STE-2 band intensity (green triangle), and the total emission intensity (blue square). The total intensity is almost constant at temperatures below 100 K, and increased monotonically at temperatures at higher than 100 K. As the temperature increased from 100 to 300 K, the total intensity eventually reached 1.8 times the value compared to the value measured at 11 K. In contrast to the case of the total intensity, the STE-1 and STE-2 band intensity showed an

inverse correlation in the temperature ranges from 11 K to 125 K. According to the trends in the data, we speculate that it is be due to a thermally activated energy transfer from STE-2 to STE-1. In the temperature between 150 and 300 K, the band intensity of both STE-1 and STE-2 increased gradually, which is similar to the total intensity. Although the mechanism of the monotonic increase in scintillation intensity remains unclear, our analysis indicates that a two-level model is insufficient to account for the temperature dependency observed in $YAl_3(BO_3)_4$. Koshimizu et al. previously observed a similar monotonic increase in scintillation in Cs_2HfCl_6 and attributed its temperature dependence to a three-level model with emissions from two excited states [48]. Hence, at least two or three excited levels are required to explain the temperature dependence of the scintillation in the $YAl_3(BO_3)_4$. In such a model, STE-1 and STE-2 are attributed to two kinds of BO_3 units ($B(1)O_3$ and $B(2)O_3$) which possibly play an important role in the excited levels (see Figure 3d).

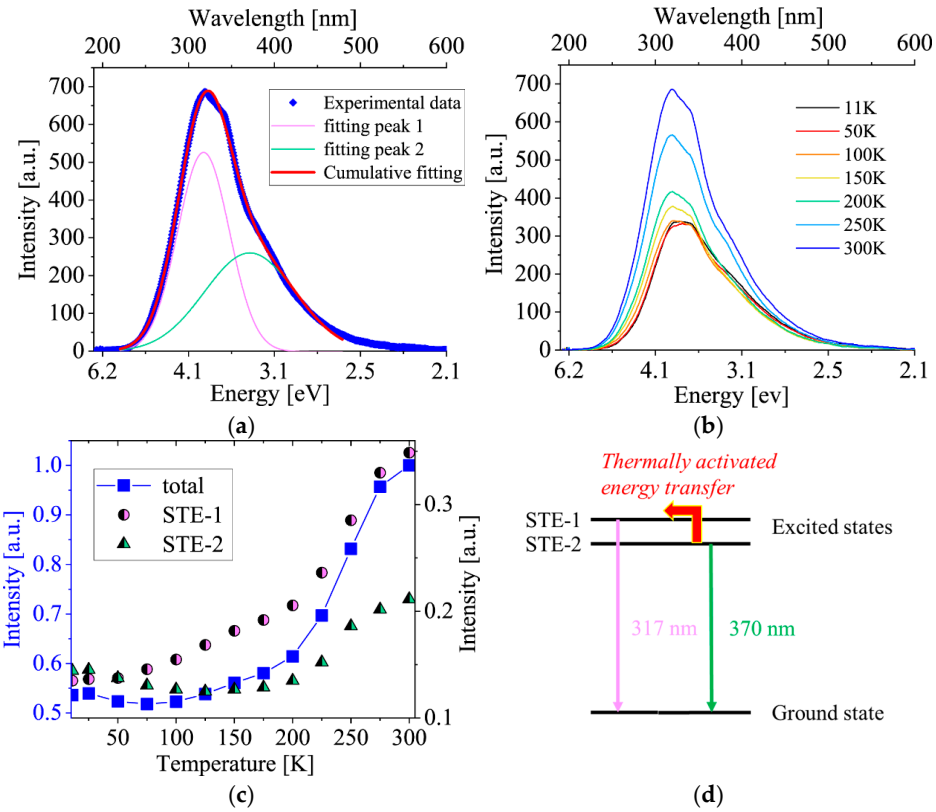


Figure 3. (**a**) X-ray excited scintillation spectrum at 300 K fitted with sums of two Gaussian functions, (**b**) the scintillation spectra at different temperatures recorded at 11, 50, 100, 150, 200, 250, and 300 K, (**c**) temperature dependence of the light yields of STE-1, STE-2 bands, and total scintillation in $YAl_3(BO_3)_4$, derived from the scintillation spectra, and (**d**) schematic diagram of proposed three-level model for the $YAl_3(BO_3)_4$.

The 5.5 MeV alpha-rays from a ^{241}Am irradiated scintillation pulse height spectrum of $YAl_3(BO_3)_4$ were evaluated, as shown in Figure 4a, which simulated neutron irradiation because the deposited secondary charged particles such as alpha and ^{7}Li particles excited the host scintillator according to the $^{10}B(n, \alpha)^7Li$ reaction. The spectrum of the GS20 measured by using a similar experimental set-up is also shown for comparison. The dominant peaks in the spectra correspond to the total absorption of alpha-particles with an energy of 5.5 MeV. The position of the peak channels was calculated by fitting with a single Gaussian function. From the calculation, the peak channels for the $YAl_3(BO_3)_4$ and GS20 were found to be about 421 and 296 channels, respectively. Thus, the scintillation light yield under alpha-rays excitation for the $YAl_3(BO_3)_4$ can be estimated to be about 140% of that

of GS20 considering the number of relative peak channels and the quantum efficiency in the 300–400 nm wavelength ranges of the PMT used as a detector. Figure 4b shows the scintillation pulse height spectra of $YAl_3(BO_3)_4$ compared with the BGO under irradiation at 662 keV gamma-rays from a ^{137}Cs. In the spectra, the ^{137}Cs-662 keV gamma-ray photopeak for the $YAl_3(BO_3)_4$ is located at the 260 channel, whereas that of the BGO is observed at the 641 channel. From the result, the scintillation light yield for the $YAl_3(BO_3)_4$ is found to be approximately 2380 photons/MeV. Taking into account the pulse height spectrum measurements, the α/β ratio is defined as follows [49].

$$\frac{\alpha}{\beta} = \frac{E_\beta}{E_\alpha} \frac{ch(E_\alpha)_\alpha}{ch(E_\beta)_\beta}$$

where $ch(E_\alpha)_\alpha$ and $ch(E_\beta)_\beta$ are the channel numbers of full absorption peaks on pulse height spectra under-irradiated at α- and β (γ)- rays, respectively. The increased α/β ratio results in a more favorable signal-to-noise ratio for neutron detection. Some neutron scintillators with a high or moderate α/β ratio have been reported previously such as LiI:Eu (α/β = 0.87), Cs_2LiYCl_6:Ce (α/β = 0.66), $Li_6Y_{0.5}Gd_{0.5}(BO_3)_3$:Ce ($\alpha/\beta$ = 0.32) [50], and GS20 (α/β = 0.3) [1,49]. Based on the calculations, the α/β ratio for $YAl_3(BO_3)_4$ is estimated to be around 0.42, which is a superior value compared to both $Li_6Y_{0.5}Gd_{0.5}(BO_3)_3$:Ce and GS20.

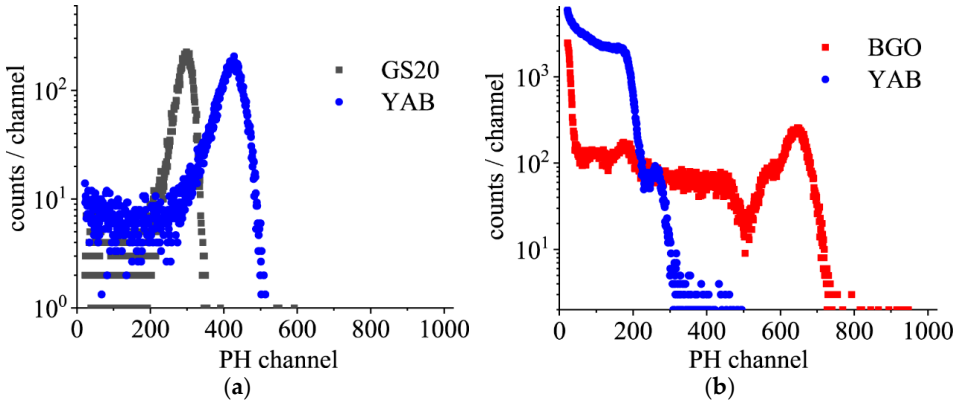


Figure 4. (**a**) ^{241}Am-alpha-ray irradiated scintillation pulse height spectra of $YAl_3(BO_3)_4$ and GS20 reference. (**b**) ^{137}Cs-gamma-ray irradiated scintillation pulse height spectra of $YAl_3(BO_3)_4$ and BGO reference.

In the concluding test as a neutron scintillator, the neutron response characteristics of $YAl_3(BO_3)_4$ were examined. Figure 5 compares the pulse height spectra of the $YAl_3(BO_3)_4$ with the GS20 under the thermal neutron exposure. In the spectra, the thermal neutron peak channels for $YAl_3(BO_3)_4$ and GS20 were the 304 channel and 675 channel, respectively. Thus, it is estimated that the scintillation light yield of the $YAl_3(BO_3)_4$ reaches 2700 photons/thermal neutron. The thermal neutron peak detected in the $YAl_3(BO_3)_4$ was associated with the Q-value of 2.31 and 2.79 MeV resulting from the $^{10}B(n, \alpha)^7Li$ reaction. In contrast, the neutron peak observed in the GS20 was attributed to the Q-value of 4.78 MeV for the $^6Li(n, \alpha)T$ reaction. For this reason, the relative light yield of the $YAl_3(BO_3)_4$ compared to GS20 differs from that estimated under 5.5 MeV alpha-ray irradiation. Compared with borate crystalline scintillators based on a $^{10}B(n, \alpha)^7Li$ reaction previously reported such as CaB_2O_4, SrB_2O_4, SrB_2O_4:Ce, and CaB_2O_4:Ce [37,38,51], the $YAl_3(BO_3)_4$ is found to have moderate light yield with a suitable scintillation wavelength for commercial PMT (see Table 1). Potentially, $YAl_3(BO_3)_4$ activated with rare-earth ions such as Ce^{3+} and Pr^{3+} should be appropriate for the development of bright neutron scintillators based on a $^{10}B(n, \alpha)^7Li$.

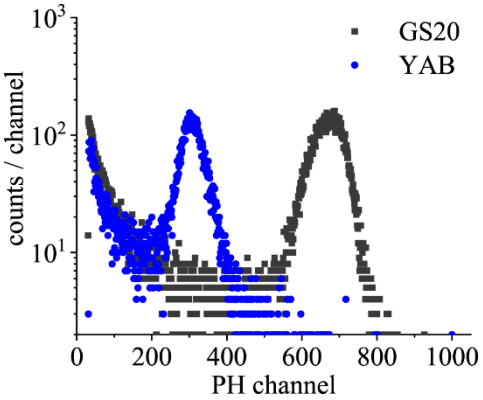


Figure 5. ^{252}Cf-neutron-irradiated scintillation pulse height spectra of $YAl_3(BO_3)_4$ and GS20 reference.

Table 1. Characteristics of $YAl_3(BO_3)_4$ compared with CaB_2O_4, SrB_2O_4, SrB_2O_4:Ce, and CaB_2O_4:Ce scintillators previously reported.

Borate Scintillator	Scintillation Wavelength [nm]	Light Yield [ph/nth]
CaB_2O_4	300–400	3200
SrB_2O_4	300, 375	1500
CaB_2O_4:Ce (0.5%)	300, 375	2200
SrB_2O_4:Ce (0.5%)	300–400	1000
$YAl_3(BO_3)_4$	**317, 370**	**2700**

4. Conclusions

In our research, we investigated the optical and scintillation properties of a $YAl_3(BO_3)_4$ single crystal prepared by the top-seeded solution growth method for a thermal neutron detector. Upon both VUV lights and X-ray excitation, the characteristic STE emission bands owing to the two kinds of BO_3 units ($B(1)O_3$ and $B(2)O_3$) were observed at 300–400 nm, which is a suitable emission wavelength for a commercial PMT. The scintillation light yield of 2700 photons/thermal neutron is smaller than that of the well-known GS20 commercial scintillator based on the ^{6}Li(n, α)^{3}H; meanwhile, the α/β ratio of 0.42 is a superior value compared with the GS20 that offers the possibility of excellent neutron/gamma-ray discrimination. The light yield achieved by making use of the $YAl_3(BO_3)_4$ is comparable to some borate scintillators based on the ^{10}B(n, α)^{7}Li previously reported. In conclusion, the properties and performance presented in this research for $YAl_3(BO_3)_4$ demonstrate that this material is a good thermal neutron scintillator host based on the ^{10}B(n, α)^{7}Li.

Author Contributions: Conceptualization, Y.F.; methodology, Y.F., M.K., K.W. and A.M.; software, H.K.; validation, Y.F., M.K. and K.A.; formal analysis, Y.F., M.K. and H.K.; investigation, Y.F., M.K. and A.M.; resources, M.K., K.W. and K.A.; data curation, Y.F., M.K. and K.W.; writing—original draft preparation, Y.F.; writing—review and editing, Y.F. and K.A.; visualization, Y.F. and H.K.; supervision, M.K. and K.A.; project administration, M.K. and K.A.; funding acquisition, Y.F., M.K. and K.A. All authors have read and agreed to the published version of the manuscript.

Funding: This study was supported by a Grant-in-Aid for Scientific Research (A) (Grant No. 22H00308, 2022–2026) and Grant-in-Aid for Challenging Research (Exploratory) (Grant No. 24K21544, 2024–2026) funded by the Japan Society for the Promotion of Science, Amano Institute of Technology 2024 research grant, Research Foundation for the Electrotechnology of Chubu 2023 research grant, a matching fund between National Institute of Advanced Industrial Science and Technology (AIST) and Tohoku University, the Cooperative Research Program of "Network Joint Research Center for

Materials and Devices" (MEXT), and Iketani Science and Technology Foundation 2024 research grant. Foundations are also acknowledged.

Data Availability Statement: The raw data supporting the conclusions of this article will be made available by the authors on request.

Conflicts of Interest: Akio Miyamoto was employed by the OXIDE Corporation. The remaining authors declare that the research was conducted in the absence of any commercial or financial relationships that could be construed as a potential conflict of interest.

References

1. van Eijk, C.W.E.; Bessière, A.; Dorenbos, P. Inorganic thermal-neutron scintillators. *Nucl. Instrum. Meth. A* **2004**, *529*, 260–267. [CrossRef]
2. Kouzes, R.T.; Ely, J.H.; Erikson, L.E.; Kernan, W.J.; Lintereur, A.T.; Siciliano, E.R.; Stephens, D.L.; Stromswold, D.C.; Ginhoven, R.M.V.; Woodring, M.L. Neutron detection alternatives to ^{3}He for national security applications. *Nucl. Instrum. Meth. A* **2010**, *623*, 1035–1045. [CrossRef]
3. Trombetta, D.M.; Klintefjord, M.; Axell, K.; Cederwall, B. Fast neutron and γ-ray coincidence detection for nuclear security and safeguards applications. *Nucl. Instrum. Meth. A* **2019**, *927*, 119–124. [CrossRef]
4. Piscitelli, F.; Mauri, G.; Laloni, A.; Hall-Wilton, R. Verification of He-3 proportional counters' fast neutron sensitivity through a comparison with He-4 detectors. *Eur. Phys. J. Plus* **2020**, *135*, 577. [CrossRef]
5. Pozzi, S.; Clarke, S.; Paff, M.; Di Fulvio, A.; Kouzes, R. Comparative neutron detection efficiency in He-3 proportional counters and liquid scintillators. *Nucl. Instrum. Meth. A* **2019**, *929*, 107–112. [CrossRef]
6. Nelson, K.A.; Bellinger, S.L.; Montag, B.W.; Neihart, J.L.; Riedel, T.A.; Schmidt, A.J.; McGregor, D.S. Investigation of a lithium foil multi-wire proportional counter for potential ^{3}He replacement. *Nucl. Instrum. Meth. A* **2012**, *669*, 79–84. [CrossRef]
7. Murray, R. Use of Li6I(Eu) as a scintillation detector and spectrometer for fast neutrons. *Nucl. Instrum.* **1958**, *2*, 237–248. [CrossRef]
8. Firk, F.W.K.; Slaughter, G.G.; Ginther, R.J. Improved Li^{6}-Loaded Glass Scintillator for Neutron Detection. *Nucl. Instrum. Methods* **1961**, *13*, 313–316. [CrossRef]
9. Knitel, M.J.; Dorenbos, P.; de Haas, J.T.M.; van Eijk, C.W.E. $LiBaF_3$, a thermal neutron scintillator with optimal n-γ discrimination. *Nucl. Instrum. Methods Phys. Res. A* **1996**, *374*, 197–201. [CrossRef]
10. Yanagida, T.; Kawaguchi, N.; Fujimoto, Y.; Fukuda, K.; Yokota, Y.; Yamazaki, A.; Watanabe, K.; Pejchal, J.; Uritani, A.; Iguchi, T.; et al. Basic study of Europium doped $LiCaAlF_6$ scintillator and its capability for thermal neutron imaging application. *Opt. Mater.* **2011**, *33*, 1243–1247. [CrossRef]
11. Iwanowska, J.; Swiderski, L.; Moszynski, M.; Yanagida, T.; Yokota, Y.; Yoshikawa, A.; Fukuda, K.; Kawaguchi, N.; Ishizu, S. Thermal neutron detection with Ce^{3+} doped $LiCaAlF_6$ single crystals. *Nucl. Instrum. Meth. A* **2011**, *652*, 319–322. [CrossRef]
12. Yanagida, T.; Kawaguchi, N.; Fujimoto, Y.; Fukuda, K.; Watanabe, K.; Yamazaki, A.; Uritani, A. Scintillation properties of LiF–SrF_2 and LiF–CaF_2 eutectic. *J. Lumin.* **2013**, *144*, 212–216. [CrossRef]
13. Trojan-Piegza, J.; Glodo, J.; Sarin, V.K. $CaF_2(Eu^{2+})$:LiF—Structural and spectroscopic properties of a new system for neutron detection. *Radiat. Meas.* **2010**, *45*, 163–167. [CrossRef]
14. Fujimoto, Y.; Kamada, K.; Yanagida, T.; Kawaguchi, N.; Kurosawa, S.; Totsuk, D.; Fukuda, K.; Watanabe, K.; Yamazaki, A.; Yokota, Y.; et al. Lithium Aluminate Crystals as Scintillator for Thermal Neutron Detection. *IEEE Trans. Nucl. Sci.* **2012**, *59*, 2252–2255. [CrossRef]
15. Yanagida, T.; Fujimoto, Y.; Koshimizu, M.; Kawano, N.; Okada, G.; Kawaguchi, N. Comparative Studies of Optical and Scintillation Properties between $LiGaO_2$ and $LiAlO_2$ Crystals. *J. Phys. Soc. Jpn.* **2017**, *86*, 094201. [CrossRef]
16. Bessiere, A.; Dorenbos, P.; van Eijk, C.W.E.; Krämer, K.W.; Güdel, H.U. Luminescence and scintillation properties of Cs_2LiYCl_6:Ce for γ and neutron detection. *Nucl. Instrum. Methods Phys. Res. A* **2005**, *537*, 242–246. [CrossRef]
17. Hawrami, R.; Ariesanti, E.; Wei, H.; Finkelstein, J.; Glodo, J.; Shah, K. Tl_2LiYCl_6: Large Diameter, High Performing Dual Mode Scintillator. *Cryst. Growth Des.* **2017**, *17*, 3960–3964. [CrossRef]
18. Kawaguchi, N.; Kawano, N.; Okada, G.; Yanagida, T. Luminescence and Scintillation Properties of LiF:W Single Crystal for Thermal-Neutron Detection. *Sens. Mater.* **2017**, *29*, 1431–1438.
19. Song, Z.; Wang, J.; Tong, Y.; Zhang, Y.; Wang, Q.; Wang, C.; Ren, G.; Sun, X.; Wu, Y. Enhancement of alpha/beta ratio in NaI:Tl,^{6}Li neutron-gamma scintillators by rare earth co-doping. *Nucl. Instrum. Methods Phys. Res. A* **2024**, *1064*, 169451. [CrossRef]
20. Xie, A.; Hettiarachchi, C.; Maddalena, F.; Witkowski, M.E.; Makowski, M.; Drozdowski, W.; Arramel, A.; Wee, A.T.S.; Springham, S.V.; Vuong, P.Q.; et al. Lithium-doped two-dimensional perovskite scintillator for wide-range radiation detection. *Commun. Mater.* **2020**, *1*, 37. [CrossRef]

21. Quang, N.D.; Vuong, P.Q.; Luan, N.T.; Truc, L.T.; Ton, N.D.; Kang, S.; Park, H.; Nam, U.-W.; Park, W.-K.; Sohn, J.; et al. Growth and characterization of ^{6}LiI:Ag crystal scintillators for thermal and epithermal neutron detection on the lunar surface. *J. Cryst. Growth* **2024**, *635*, 127692. [CrossRef]
22. Yuan, D.; Víllora, E.G.; Kawaguchi, N.; Nakauchi, D.; Kato, T.; Yanagida, T.; Shimamura, K. Thermal neutron scintillation improvement in Ce:$Li_6Y(BO_3)_3$ single crystals by thermal treatment. *Jpn. J. Appl. Phys.* **2023**, *62*, 010614. [CrossRef]
23. Wang, Q.; Wang, C.; Wang, Z.; Sun, X.; Nikl, M.; OuYang, X.; Wu, Y. Achieving Efficient Neutron and Gamma Discrimination in a Highly Stable ^{6}Li-Loaded $Cs_3Cu_2I_5$ Perovskite Scintillator. *J. Phys. Chem. Lett.* **2022**, *13*, 9066–9071. [CrossRef]
24. Nasir, R.; Aziz, F.; Mirza, S.M.; Mirza, N.M. Experimental and theoretical study of BF_3 detector response for thermal neutrons in reflecting materials. *Nucl. Eng. Technol* **2018**, *50*, 439–445. [CrossRef]
25. Amaro, F.D.; Monteiro, C.M.B.; dos Santos, J.M.F.; Antognini, A. Novel concept for neutron detection: Proportional counter filled with ^{10}B nanoparticle aerosol. *Sci. Rep.* **2017**, *7*, 41699. [CrossRef] [PubMed]
26. Ballman, A.A. A new series of synthetic borates isostructural with the carbonate mineral huntite. *Am. Mineral.* **1962**, *47*, 1380–1383.
27. Mills, A.D. Crystallographic Data for New Rare Earth Borate Compounds, $RX_3(BO_3)_4$. *Inorg. Chem.* **1962**, *1*, 960–961. [CrossRef]
28. Fan, M.; Wu, G.; Chen, F.; Yu, F.; Cheng, X.; Zhao, X. Electro-elastic features of Nd-doped $YAl_3(BO_3)_4$ single crystal. *Cryst. Eng. Comm.* **2020**, *22*, 7816–7825. [CrossRef]
29. Li, J.; Wang, J.; Cheng, X.; Hu, X.; Burns, P.; Dawes, J. Thermal and laser properties of Yb:$YAl_3(BO_3)_4$ crystal. *J. Cryst. Growth* **2003**, *250*, 458–462. [CrossRef]
30. Yokosawa, N.; Suzuki, K.; Nakazawa, E. Vacuum ultraviolet excitation processes of $YAl_3(BO_3)_4$: R (R = Eu^{3+}, Gd^{3+} and Tb^{3+}). *Jpn. J. Appl. Phys.* **2003**, *42*, 5656–5659. [CrossRef]
31. Yoshida, H.; Yoshimatsu, R.; Watanabe, S.; Ogasawara, K. Optical Transitions near the Fundamental Absorption Edge and Electronic Structures of $YAl_3(BO_3)_4$:Gd^{3+}. *Jpn. J. Appl. Phys.* **2006**, *45*, 146–151. [CrossRef]
32. Cavalli, E.; Bovero, E.; Magnani, N.; Ramirez, M.O.; Speghini, A.; Bettinelli, M. Optical spectroscopy and crystal-field analysis of $YAl_3(BO_3)_4$ single crystals doped with dysprosium. *J. Phys. Condens. Matter* **2003**, *15*, 1047–1056. [CrossRef]
33. Dominiak-Dzik, G.; Ryba-Romanowski, W.; Kovács, L.; Beregi, E. Effect of temperature on luminescence and VUV to visible conversion in the $YAl_3(BO_3)_4$:Dy^{3+} (YAB:Dy) crystal. *Radiat. Meas.* **2004**, *38*, 557–561. [CrossRef]
34. Bartl, M.H.; Gatterer, K.; Cavalli, E.; Speghini, A.; Bettinelli, M. Growth, optical spectroscopy and crystal field investigation of $YAl_3(BO_3)_4$ single crystals doped with tripositive praseodymium. *Spectrochim. Acta Part A* **2001**, *57*, 1981–1990. [CrossRef]
35. Aloui-Lebbou, O.; Goutaudier, C.; Kubota, S.; Dujardin, C.; Cohen-Adad, M.T.; Pédrini, C.; Florian, P.; Massiot, D. Structural and scintillation properties of new Ce^{3+}-doped alumino-borate. *Opt. Mater.* **2001**, *16*, 77–86. [CrossRef]
36. Feofilov, S.; Zhou, Y.; Jeong, J.; Keszler, D.; Meltzer, R. Energy transfer from the host excitations to Ce^{3+} ions in scandium borate. *J. Lumin.* **2007**, *125*, 80–84. [CrossRef]
37. Fujimoto, Y.; Yanagida, T.; Yokota, Y.; Kawaguchi, N.; Fukuda, K.; Totsuka, D.; Watanabe, K.; Yamazaki, A.; Yoshikawa, A. Growth and characterization of strontium metaborate scintillators. *Opt. Mater.* **2011**, *34*, 444–447. [CrossRef]
38. Fujimoto, Y.; Yanagida, T.; Kawaguchi, N.; Fukuda, K.; Totsuka, D.; Watanabe, K.; Yamazaki, A.; Chani, V.; Nikl, M.; Yoshikawa, A. Crystal growth and characterization of calcium metaborate scintillators. *Nucl. Instrum. Methods Phys. Res. A* **2013**, *703*, 7–10. [CrossRef]
39. Yanagida, T.; Kimura, H.; Nakauchi, D.; Kato, T.; Kawaguchi, N. Photoluminescence and scintillation characteristics of b-BaB_2O_4 single crystal. *Jpn. J. Appl. Phys.* **2020**, *59*, 102004. [CrossRef]
40. Kawaguchi, N.; Okada, G.; Futami, Y.; Nakauchi, D.; Kato, T.; Yanagida, T. Scintillation and Dosimetric Properties of Monocrystalline and Polycrystalline $Li_2B_4O_7$. *Sens. Mater.* **2020**, *32*, 1419–1426. [CrossRef]
41. Fukui, K.; Miura, H.; Nakagawa, H.; Shimoyama, I.; Nakagawa, K.; Okamura, H.; Nanba, T.; Hasumoto, M.; Kinoshita, T. Performance of IR-VUV normal incidence monochromator beamline at UVSOR. *Nucl. Instrum. Methods Phys. Res. A* **2001**, *467–468*, 601–604. [CrossRef]
42. Koshimizu, M.; Onodera, K.; Nishikido, F.; Haruki, R.; Shibuya, K.; Kishimoto, S.; Asai, K. X-ray detection capability of a $BaCl_2$ single crystal scintillator. *J. Appl. Phys.* **2012**, *111*, 024906. [CrossRef]
43. Yanagida, T.; Fujimoto, Y.; Yagi, H.; Yanagitani, T. Optical and scintillation properties of transparent ceramic Yb:Lu_2O_3 with different Yb concentrations. *Opt. Mater.* **2014**, *36*, 1044–1048. [CrossRef]
44. Moszyixki, M.; Kapusta, M.; Mayhugh, M.; Wolski, D.; Flyckt, S.O. Absolute light output of scintillators. *IEEE Trans. Nucl. Sci.* **1997**, *44*, 1052–1061. [CrossRef]
45. van Eijk, C.W.E. Inorganic Scintillators for Thermal Neutron Detection. *Rad. Meas.* **2004**, *38*, 337–342. [CrossRef]
46. Yu, X.; Yue, Y.; Yao, J.; Hu, Z.-G. $YAl_3(BO_3)_4$: Crystal growth and characterization. *J. Cryst. Growth* **2010**, *312*, 3029–3033. [CrossRef]
47. Yoshida, H.; Fujikawa, K.; Toyoshima, H.; Watanabe, S.; Ogasawara, K. Luminescence properties of $YAl_3(BO_3)_4$ substituted with Sc^{3+} ions. *Phys. Stat. Sol. A* **2006**, *203*, 2701–2704. [CrossRef]
48. Koshimizu, M.; Saeki, K.; Fujimoto, Y.; Okada, G.; Yanagida, T.; Yamashita, S.; Asai, K. A three-state model for describing the temperature variation of the scintillation properties of Cs_2HfCl_6. *Jpn. J. Appl. Phys.* **2018**, *57*, 032401. [CrossRef]

49. Wolszczak, W.W.; Dorenbos, P. Nonproportional Response of Scintillators to Alpha Particle Excitation. *IEEE Trans. Nucl. Sci.* **2017**, *64*, 1580–1591.
50. Fawad, U.; Rooh, G.; Kim, H.J.; Park, H.; Kim, S.; Khan, S. Scintillation properties of $Li_6Y_{0.5}Gd_{0.5}(BO_3)_3$: Ce^{3+} single crystal. *J. Cryst. Growth* **2015**, *410*, 18–22. [CrossRef]
51. Fujimoto, Y.; Yanagida, T.; Kawaguchi, N.; Kurosawa, S.; Fukuda, K.; Totsuka, D.; Watanabe, K.; Yamazaki, A.; Yokota, Y.; Yoshikawa, A. Characterizations of Ce^{3+}-Doped CaB_2O_4 Crystalline Scintillator. *Cryst. Growth Des.* **2012**, *12*, 142–146. [CrossRef]

Disclaimer/Publisher's Note: The statements, opinions and data contained in all publications are solely those of the individual author(s) and contributor(s) and not of MDPI and/or the editor(s). MDPI and/or the editor(s) disclaim responsibility for any injury to people or property resulting from any ideas, methods, instructions or products referred to in the content.